Jinst

Published by IOP Publishing for Sissa Medialab

Received: *December 19, 2019*
Revised: *January 13, 2020*
Accepted: *January 16, 2020*
Published: *February 11, 2020*

Measurement of mass and total kinetic energy distribution of fission fragments using newly developed compact MWPC detectors

A. Pal,[a,b] **S. Santra,**[a,b,1] **A. Kundu,**[a,b] **D. Chattopadhyay,**[a,b] **A. Jhingan,**[c] **B.K. Nayak**[a,b] **and S. Prafulla**[d]

[a] *Nuclear Physics Division, Bhabha Atomic Research Centre, Mumbai, 400085, India*
[b] *Homi Bhabha National Institute, Anushaktinagar, Mumbai, 400094, India*
[c] *Inter University Accelerator Centre, Aruna Asaf Ali Marg, New Delhi, 110067, India*
[d] *Electronics Division, Bhabha Atomic Research Centre, Mumbai, 400085, India*

E-mail: ssantra@barc.gov.in

Abstract: Two large area (12.5 cm × 7.5 cm) position sensitive compact multiwire proportional counter detectors have been developed for the study of fission reactions for bombarding energies near the Coulomb barrier. Each detector provides one negative fast signal (anode signal) which is used for the time of flight measurement, in addition to four position signals. The timing signal from anode and delayed timing signal from position frames are processed through non-inverting and inverting fast preamplifiers developed in-house. These preamplifiers are based on monolithic microwave integrated circuits. The position resolutions were measured using a mask made of aluminium. The X and Y-position resolutions were found to be ≈ 1.3 and 1.4 mm respectively. The time spread obtained from the sum spectra of position signals extracted from both the ends of the same position frame, was ≈ 1.6 ns. The detectors were used successfully in an in-beam experiment to detect the fission fragments in the ^{19}F+^{238}U reaction. The time correlation spectra between two anode signals provide clean identification of fission events. Difference of those recorded time was used to measure the mass distribution and hence the total kinetic energy distribution of the fission fragments.

Keywords: Instrumentation and methods for heavy-ion reactions and fission studies; Timing detectors

[1] Corresponding author.

https://doi.org/10.1088/1748-0221/15/02/P02008

2020 JINST 15 P02008

Contents

2020 JINST 15 P02008

1 Introduction

In the recent past, there is immense interest to study fission reactions following heavy ion induced fusion and transfer reactions because of its fundamental and application oriented importance [1–8]. Emphasis has been given on transfer induced fission as it can be utilized to study fission dynamics of neutron rich nuclei which can not be populated using stable target and projectiles and also to determine neutron induced fission cross-sections useful for fast reactors using surrogate techniques. However, these kind of measurements are challenging as they require clean identification of fission events and also large angular coverage of detectors to detect the fission fragments.

Conventionally, the silicon detectors are used for the detection of light charged particles. However, for heavy particles like fission fragments, these are not suitable due to their fast degradation of performance with radiation damage and small geometrical efficiency. Large area position sensitive silicon detectors are commercially available not only at high cost but also with limited sustainability when used for fission fragments. Another serious disadvantage of a silicon detector is its inability to distinguish fission fragments from elastic and quasielastic particles at higher energies for heavy beams like ^{19}F,^{32}S etc. To overcome the above problems, other detectors such as position sensitive micro channel plates 'CORSET' gas ionization chambers, and proportional counters have been developed. Large area micro channel plate system is difficult to develop and is generally fragile. Gas ionization chambers have poor count rate handling capabilities, and also have poor timing, position, and energy resolutions.

The multi-wire proportional counter (MWPC) detectors have been an efficient solution to the above problems which provide very good timing and position resolutions, higher count rate handling capability and also insensitivity to radiation damage. They can also be fabricated easily with various sizes according to the need for experimental investigations. Moreover, the operating parameters such as gas pressures and voltages on electrodes can be adjusted to make it transparent to unwanted light particles and make it sensitive only to heavier particles such as fission fragments. Although

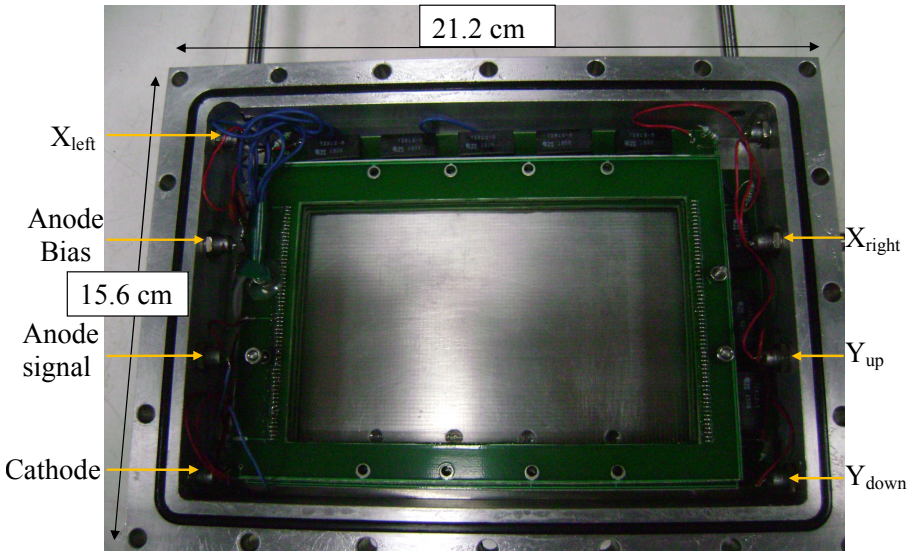

Figure 1. (Color online) The inside-out of the MWPC detector cavity containing 5 PCB frames and 7 feedthrus for signals and bias supplies.

energy resolution of the detector is very poor, it provides a clear distinction between light and heavy charged particles.

The development of gas detectors was truly revolutionized by the invention of the MWPC [9] by Georges Charpak in 1968. Later Amos Breskin developed a detector (known as Breskin detector) [10, 11] which consisted of a pre-amplification stage operating as a parallel plate chamber (PPAC) directly coupled to a MWPC. Subsequently, several experimental groups [12–14] have developed MWPC detectors with different sizes as per their requirement. To understand fission dynamics near Coulomb barrier, we have also developed two compact MWPC detectors for the detection of fission fragments, which are similar to Breskin detectors. Each of the detectors are having identical dimensions, design features and performances. It consists of 5 PCB frames (2 cathodes, 1 anode, 1 X-position frame and 1 Y-position frame) and there are 7 LEMO feedthrus as shown in figure 1. Both the cathode frames are electrically shorted and connected to a single LEMO connector through which the bias voltage is supplied as well as the signal is collected with the help of a charge sensitive pre-amplifier. There are two separate connections for the anode frame: one for supplying bias and the other for extracting the signal. The X-position frame has two connections: the X_{left} and X_{right}. Similarly, two output connections (Y_{up} and Y_{down}) have been taken from the Y-position frame. It may be mentioned that the detectors can also be used with 4 plate geometry with one less number of cathode. The detectors have been successfully tested using fission sources as well as with in-beam experiments. The descriptions of the detailed design and the results of the test performances are as follows.

2 Detector design and construction

The detector has been designed based on the requirements that it should (i) provide good position ($\sim$ 1.5 mm) and timing ($\sim$ 1 ns) resolutions (ii) provide a reasonably good angular coverage

2020 JINST 15 P02008

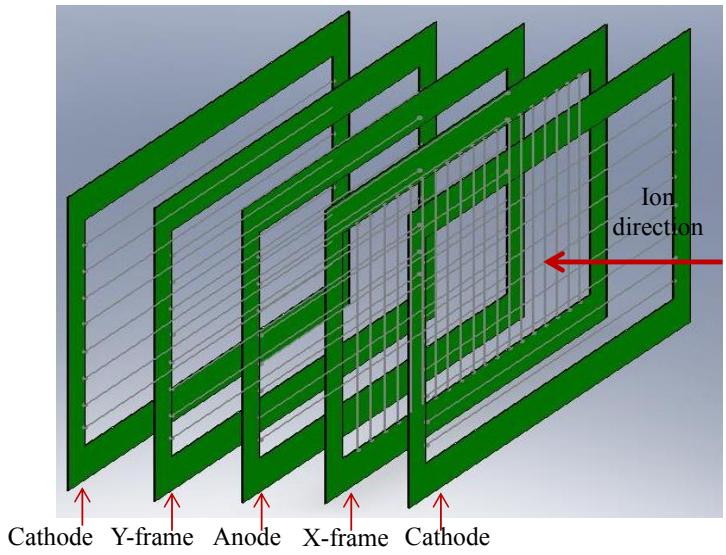

Figure 2. (Color online) Schematic diagram showing the arrangement of different PCB frames inside the MWPC detector.

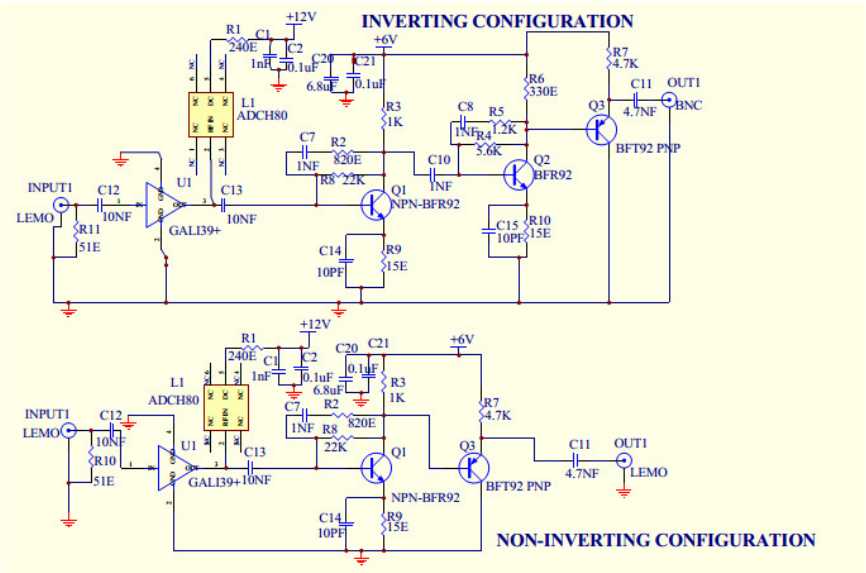

Figure 3. (Color online) Schematic diagram showing the designs of the newly developed inverting as well as non-inverting fast preamplifiers based on Monolithic Microwave Integrated Circuits.

and (iii) be compact in order to be placed at extreme backward angles without blocking the beam direction. The design, similar to the one developed by Breskin [11], can fulfill the above criteria.

The core of the detector consists of five frames each with an active area $12.5 \times 7.5\,\mathrm{cm}^2$. As shown in figure 2, the arranged wire frames starting from the entrance of the detector are: a cathode, an X-frame, an anode, a Y-frame and a second cathode (shorted with the first cathode). Such a design provides high gain for both heavy and light ions at low gas pressure [$\sim$ 1–5 torr]. All wire frames are made from gold plated tungsten wire with 20 µm diameter, stretched on a 1.6 mm thick

2020 JINST 15 P02008

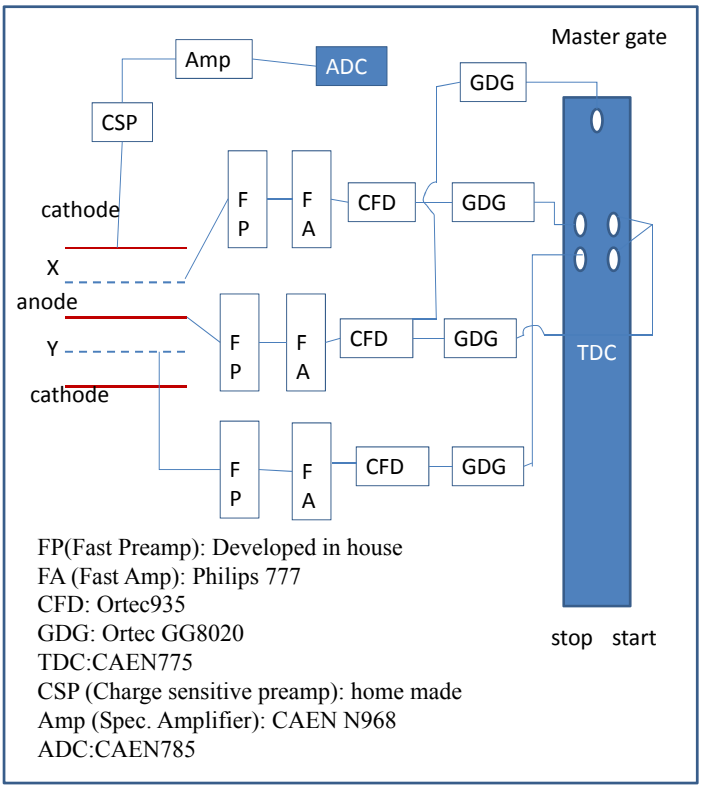

Figure 4. (Color online) Schematic diagram of the electronic circuit used for data acquisition during a typical off-line detector test using a fission source.

printed circuit board. All the frames are stacked one after another. The X frame is made from 100 wires whereas the remaining frames have 60 wires each. The separation of two consecutive wires is 1.27 mm. Using commercially available rhombus delay line integrated chips (model TZB12-5) position information from X and Y frames are extracted. In position electrodes, wires are shorted in pair and connected to one tap of delay line chip. End to end delay in X and Y-position frames are 100 and 60 ns, respectively. The position frames are kept at ground potential by terminating both ends of delay lines through 150 kΩ resistors. The electrode assembly is mounted inside a rectangular metal housing milled out from a solid aluminum block of dimension 21.2 cm × 15.6 cm. At the entrance of the detector 0.5 μm thick mylar foil has been used to isolate it from the vacuum chamber. The foil is supported by nylon wire. The detector is operated with flowing isobutane gas at ∼ 1–4 torr pressure.

3 Electronics for pulse processing

The MWPC detector consists of multiple wires where each wire acts as a cylindrical proportional counter. It is well known that the electric field intensity at a given pressure is the highest in the region very near to the anode, which is mainly responsible for the avalanche caused by the primary electrons produced in the region between cathode and sense wires. Once the avalanche is produced, electrons and ions will move towards anode and cathode respectively. As the travel path for electron

2020 JINST 15 P02008

is very short, it will contribute very less (< 1%) to the signal. It is therefore the movement of the positive ions which is responsible for inducing a fast measurable negative signal at anode and fast measurable positive pulses at position sensing wires. The position signals will travel through delay line chips and are to be collected from the two ends of the frames. Therefore we are supposed to get 4 positive pulses from two position frames and one negative pulse from the anode frame. Now the challenge is to process both the positive and negative pulses simultaneously for acquisition through preamplifiers. The positive pulses are needed to be inverted to feed into the Constant Fraction Discriminator (CFD) module. Therefore it requires four inverting and one non-inverting preamplifiers. Both inverting and non-inverting wide-band voltage sensitive preamplifiers made of transistors (ORTEC VT120) are available in the market. Each preamplifier is having single channel only. Hence it requires 5 separate preamplifiers for each MWPC detector. But, for the present work, a compact low noise fast pre amplifier having one non-inverting and 4 inverting channels together has been designed. The design for inverting and non-inverting channels are separately shown in figure 3. Two such preamplifiers were developed for the two MWPC detectors. The commercially available fast preamplifiers are generally made of transistors only. However, the presently designed pre-amplifiers are based on Monolithic Microwave Integrated Circuits (MMIC). We have used GALI 39^{+} MMIC, which is a wide-band amplifier offering high dynamic range. This uses Darlington configuration and is internally matched to 50 ohms. To increase the gain further, additional transistor stages have also been used at the output of this IC.

The output signals obtained from the preamplifiers are further processed through various modules as shown in figure 4. The additional gain required for signals obtained from preamplifiers are supplied through fast amplifiers (PHILIPS 777). All the timing signals are fed into CFD (ORTEC935) to generate NIM logic pulses. After adjusting the timing delay using the Gate and Delay Generator (GDG) module (ORTEC GG8020) one can use anode as START and position signals as STOP signals for timing measurements. The anode signal is also used as the master trigger for the data acquisition system. The cathode signal which is a measure of energy deposition in the active volume of the detector is read out by a low gain charge sensitive preamplifier built in-house.

4 Detector performance testing

The detectors have been tested with ^{252}Cf fission source as well as with in-beam experiment. For fission fragment detection, the bias voltages of +360 V and −170 V were supplied to anode and cathode respectively when there were five frames inside the detector chamber. With four plates geometry, we optimized the detector performance by setting the anode voltage at +420 V and the cathode voltage at −80 V to get its best timing and position resolution. The detector was operated with flowing isobutane gas at ∼ 3 torr pressure. The test results obtained using fission source as well as using heavy ion beam are discussed below.

4.1 With source

As discussed in the previous section, four positive pulses and one negative pulse are processed through 4 inverting and one non-inverting channels to make all the signals of negative polarity. The images for two position signals and one anode signal are indeed observed as negative polarity

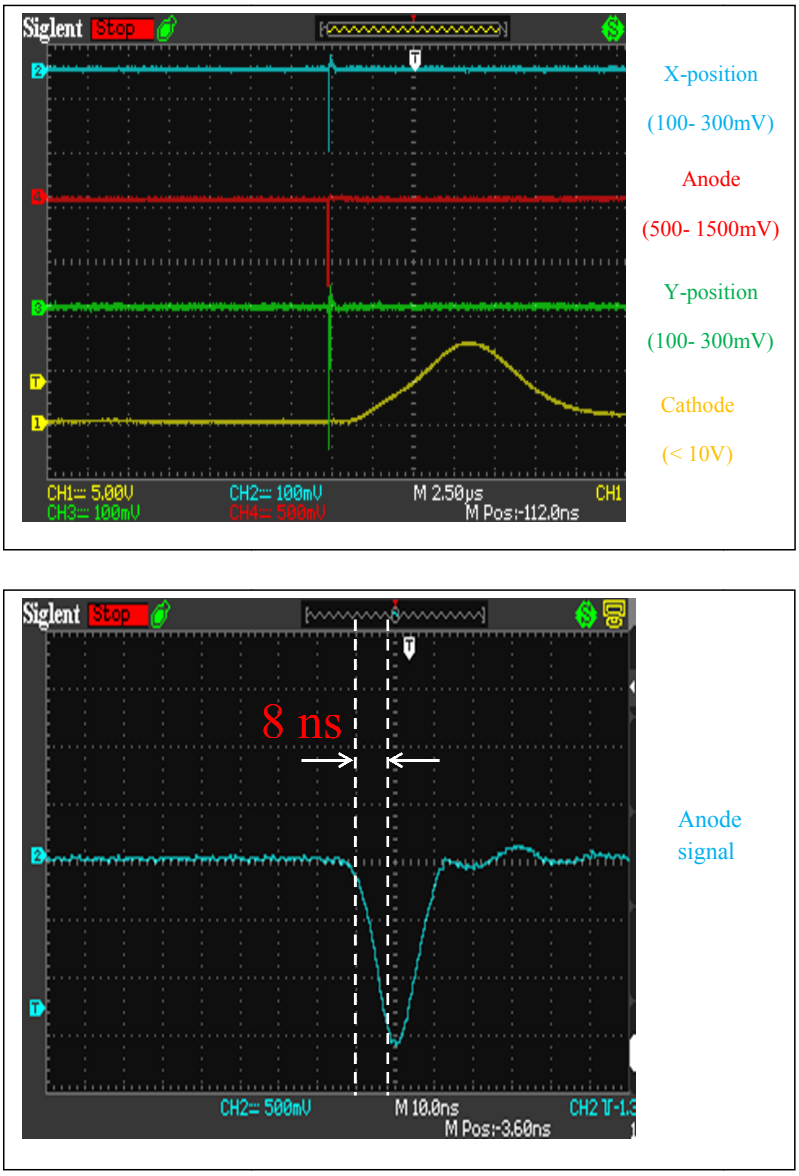

Figure 5. (Color online) (Top panel) Pre-amplifier output signals observed in an oscilloscope corresponding to x position (cyan), anode (red), y position (green) and cathode (yellow) signals, and (bottom panel) the zoomed-in view of the anode signal showing the rise time of ~ 8 ns.

signal in oscilloscope as shown in figure 5. The pulse height of anode signal of 500–1500 mV was observed with a rise time less than 10 ns as shown in figure 5. Typical pulse height of 100–300 mV was observed for each of the position signals. It is further amplified by a fast amplifier (PHILIPS 777) before feeding into CFD. The pulse height of the cathode signal was observed in the range of 1–10 V when the output of the low gain charge sensitive preamplifier is fed into a linear amplifier. The recorded cathode spectrum as shown in figure 6 shows a clear distinction between alpha particles and fission fragments.

2020 JINST 15 P02008

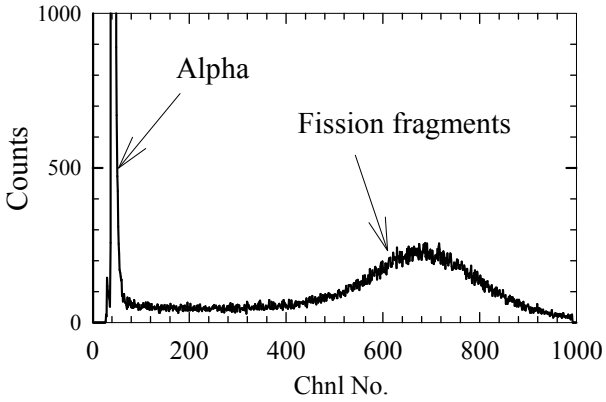

Figure 6. A typical spectrum obtained by acquiring the Cathode signal using a low-gain charge-sensitive pre-amplifier (built in-house) during an off-line test, showing clear distinction between α particles and fission fragments.

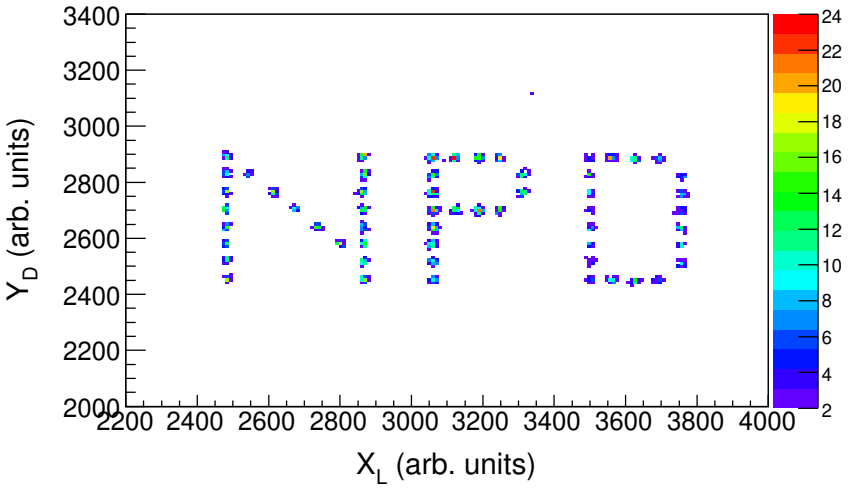

Figure 7. (Color online) A two dimensional pattern obtained from the spectra of X_{left} versus Y_{down} acquired during the detector test using a fission source while placing an aluminium mask (with holes of exactly the same pattern) in front of the detector.

To determine position resolution, an aluminium mask with holes of 1 mm diameter with a separation of 5 mm between two adjacent holes was placed in front of the detector at a distance of $\sim$ 30 cm from the source and the mask is at $\sim$ 2 cm from the first electrode. As shown in figure 7, the projection of the mask on the detector is reproduced hole by hole in the two dimensional spectrum when we plot the spectrum of X_{left} versus Y_{down}. Some holes were deliberately blocked to create the shown pattern. The X and Y projections of the mask on the detector have been shown in figure 8(a) and (b) respectively, where peak to peak separation is 5 mm. The average FWHM of the peaks for X frames have been found to be $\sim$ 1.3 mm. Similarly the average FWHM of $\sim$ 1.4 mm has been obtained from the Y projections of the above 2-D spectra. Slightly broader FWHM of the Y positions are due to the location of the Y wire frame at larger distance from the source, compared to the X wire frame. Thus the projection of the hole on the Y wire frame is likely to be more magnified as compared to X.

2020 JINST 15 P02008

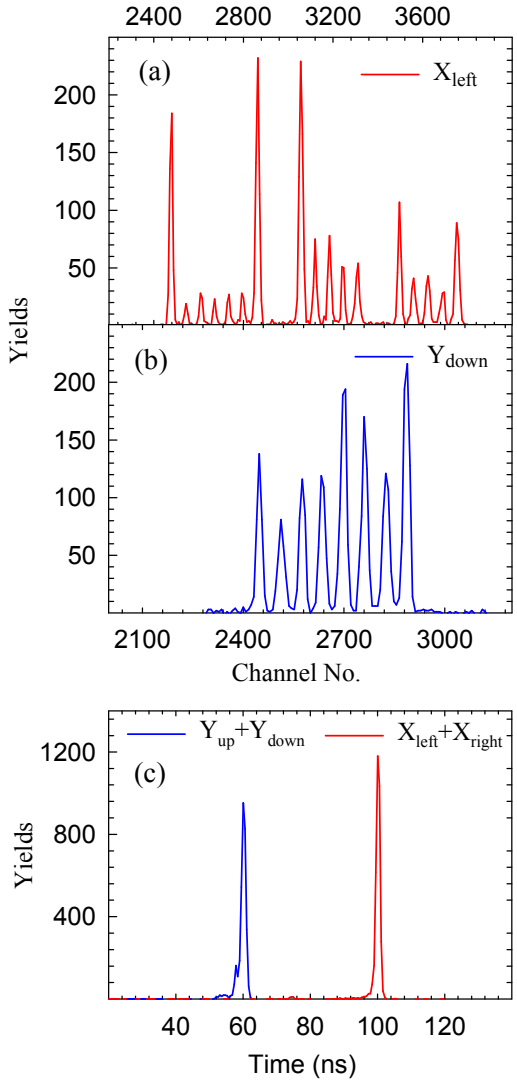

Figure 8. (Color online) Typical position spectra recorded using ^{252}Cf fission source correspond to: (upper panels) the signals of X-left, i.e., 'X_L' (red solid line) and Y-down, i.e., 'Y_D' (blue solid line), and (lower panel) sum of both signals of x position, i.e., '$X_L + X_R$' (red solid line) and sum of both signals of y positions, i.e., '$Y_U + Y_D$' (blue solid line) respectively.

From the individual spectra of X_{left}, X_{right}, Y_{up} and Y_{down}, one get the x,y position information of an event. However, if we record all the signals simultaneously, one can obtain x position spectrum by taking the difference between X_{left} and X_{right} (i.e. $X_L - X_R$). Similarly, y position can be obtained by taking the difference between Y_{up} and Y_{down} (i.e. $Y_U - Y_D$). Interestingly the sum of the position signals (X_L+X_R) and (Y_U+Y_D) should be equal to the total delay of the delay line which should remain constant. This is used to eliminate events arising from reflections and pickups in delay lines and transmission cables, weak signals which are triggered by CFD on one side but not on the other side, and multiple hit events. While tuning electronics these widths are monitored to get the best possible width as narrow as possible. The width of these peaks is a measure of the time dispersion in the detector as well as electronics setup. Time dispersion of 1.6 ns in the detector as well as

2020 JINST 15 P02008

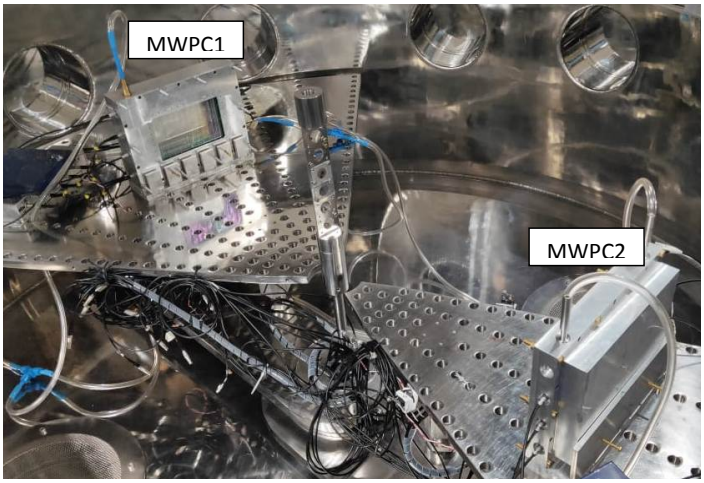

Figure 9. (Color online) An experimental setup using two MWPC detectors placed inside the General Purpose Scattering Chamber of the 0° beam line of the Pelletron Accelerator Facility, Mumbai for in-beam testing.

electronics setup has been determined from the width of the peaks of sum spectra as shown in figure 8 (c). With satisfactory test performance including position resolution and time dispersion, the detector is made ready for online fission measurements.

4.2 In-beam testing

The detectors were tested successfully with the measurements of fission fragments produced in the ^{19}F + ^{238}U reaction using general purpose scattering chamber at BARC-TIFR Pelletron-Linac facility. As shown in figure 9, two MWPC detectors (MWPC1 and MWPC2) have been placed at folding angles at a distance of 41.4 cm and 39.4 cm respectively from the target centre. Pulsed RF beams were used to get the start signal of the time-of-flight. Timing pulses from the anodes of the MWPC detectors were processed through constant fraction discriminators (CFD) and the "OR" of the discriminator pulses were taken in coincidence with the RF pulse from the beam buncher of the Pelletron accelerator through the "AND" gate. The coincident pulse is used as master trigger for the VME based data acquisition system. The anode signals and position signals from the two detectors were suitably amplified and processed through CFD to generate logic pulses which are delayed by delay units and were time analyzed by a Time to Digital Converter (TDC) Model V775. The correlations of time-of-flights for the two fission fragments have been shown in figure 10. Here, we get a clean correlation plots for the two fission fragments devoid of any quasi-elastic events. The two blobs correspond to two RF bunches which are separated by 107 ns in time. In the present setup, both the detectors are having angular coverage of $\sim (72^\circ - 88^\circ)$ in either side of the beam direction. If elastic or quasi-elastic particles are detected in one of the MWPC detectors, the corresponding recoiling heavy nuclei are not kinematically allowed to move in the direction of the second detector. Thus there will be no correlation in timing signal between light quasi-elastic particles and heavy recoiling nuclei.

2020 JINST 15 P02008

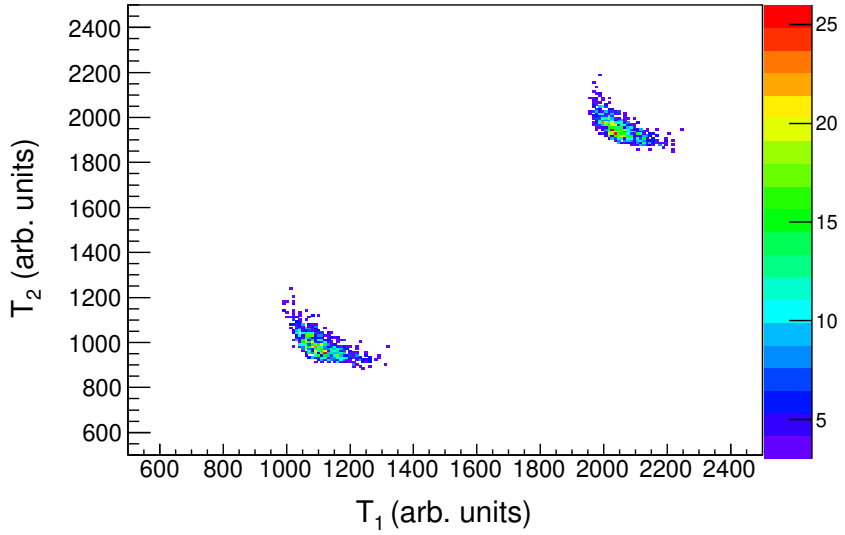

Figure 10. (Color online) The correlations of time-of-flights (T_1 versus T_2) of two fission fragments produced in ^{19}F+^{238}U reaction at E_{beam} = 107 MeV.

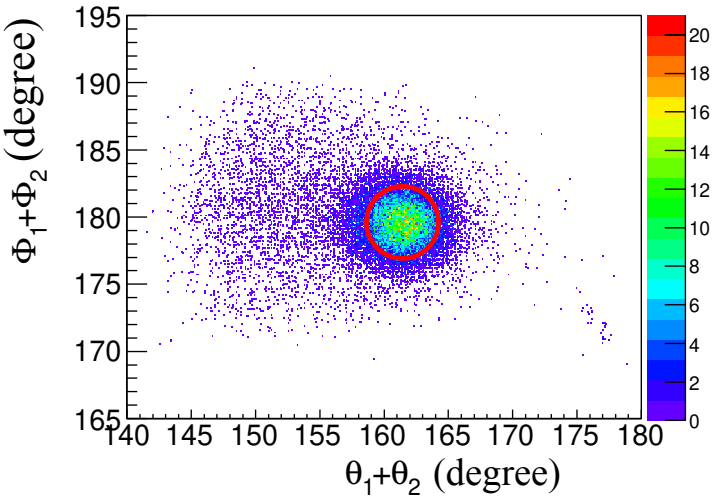

Figure 11. (Color online) A typical $\theta_1 + \theta_2$ vs. $\phi_1 + \phi_2$ plot obtained for the detected fission fragments produced in ^{19}F+^{238}U reaction at E_{beam} = 107 MeV. The events inside the red circle correspond to full momentum transfer.

4.3 Derivation of mass and total kinetic energy distribution

The fission fragment (FF) mass distributions can be directly determined by measuring velocities of the two fragments in a time of flight measurement [15]. The START time is either obtained from the pulsed beam [16] or measured using a PPAC (Parallel plate avalanche counter) or MCP (Micro Channel Plate) based detector [17–19]. The STOP time can be derived using a PPAC, MWPC and solid state detectors. Use of a silicon detector suffers from time delay and pulse defects due to plasma effects [20]. The advantage of using a pulsed beam over a start detector is that no extra energy loss correction is required for pulsed beam. For a pulsed beam the time spread of the bunched beam limits the mass resolution. Most often, time difference method is applied when pulsed beam is used [13]. The procedure to derive FF mass distribution has been described below.

2020 JINST 15 P02008

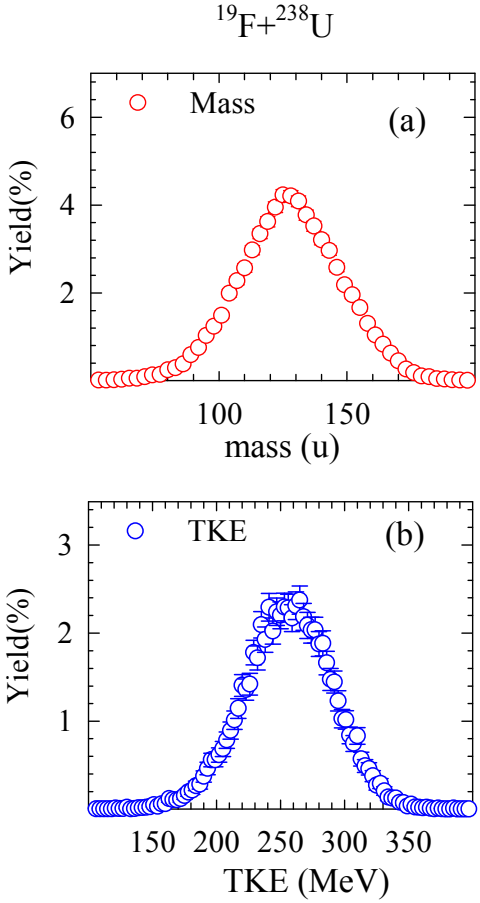

Figure 12. (Color online) Distributions of (a) mass and (b) total kinetic energy of the fission fragments produced in ^{19}F+^{238}U reaction at E_{beam} = 107 MeV.

The position spectra are calibrated using a mask with known dimensions. The timing spectra are calibrated using a time calibrator which generates two signals, one of which is used as a START and the other one as a STOP signal after providing a suitable delay. After position calibrations, the values of scattering angle (θ) and azimuthal angle (ϕ) of the fission fragments were obtained on event-by-event basis. Due to finite size of the beam spot ($\sim$ 5 mm) on the target, an uncertainty of $\sim 0.4^\circ$ or less is introduced in the calculation of the angles which further leads to an uncertainty of $\sim$ 1% in the momentum. A typical $(\theta_1+\theta_2)$ vs. $(\phi_1+\phi_2)$ plot has been obtained for ^{19}F+^{238}U reaction at 107 MeV beam energy as shown in figure 11, which shows a clear distinction between dense patch corresponding to full momentum (mainly complete fusion-fission) and the scattered points corresponding to partial momentum transfer (transfer induced fission) events. The events inside the red contour, corresponding to full momentum transfer as shown in figure 11, were analyzed to obtain the fission fragment mass distribution (FFMD).

From the difference in measured time-of-flights of two fission fragments of the same event (t_1 and t_2), one can derive masses of the fragments using the following equation as described in ref. [13].

$$m_1 = \frac{(t_1 - t_2) + \delta t_0 + m_{\text{CN}}\frac{d_2}{p_2}}{\frac{d_1}{p_1} + \frac{d_2}{p_2}} \tag{4.1}$$

2020 JINST 15 P02008

where d_1 and d_2 are the flight paths of the two fragments, m_{CN} is the mass of compound nucleus formed in the reaction, δt_0 is the electronic delay between the two detectors and p_1, p_2 are momenta of the fragments obtained from the following equation.

$$p_1 = \frac{m_{CN} v_{CN}}{\cos\theta_1 + \sin\theta_1 \cot\theta_2}$$
$$p_2 = \frac{p_1 \sin\theta_1}{\sin\theta_2}$$

The value of δt_0 should be such that mass distribution becomes symmetric around $\frac{m_{CN}}{2}$. Now the velocities in the lab-frame are obtained by dividing the momenta by the respective masses. Those velocities are transformed in the centre-of-mass frame as follows

$$v_{1cm} = \sqrt{v_1^2 + v_{cn}^2 - 2 v_1 v_{cn} \cos\theta_1}$$
$$v_{2cm} = \sqrt{v_2^2 + v_{cn}^2 - 2 v_2 v_{cn} \cos\theta_2}$$

Finally total kinetic energy (TKE) of the two fission fragments in the centre-of-mass frame are obtained from the following equation.

$$TKE = \frac{1}{2} m_1 v_{1cm}^2 + \frac{1}{2} m_2 v_{2cm}^2 \tag{4.2}$$

A typical mass distribution of the fission fragments produced in $^{19}F+^{238}U$ reaction at 107 MeV bombarding energy, obtained using equation (1) is shown in figure 12(a). Similarly a typical TKE distribution, obtained for the same reaction is shown in figure 12(b). The mass distribution is expected to be a symmetric Gaussian distribution. The same is true for the TKE distribution. The most probable value of the TKE obtained from the present measurement is more than the average value obtained from Viola systematics [21]. A mass resolution of ~ 5 a.m.u. has been achieved. In order to measure the mass and TKE distributions with good resolutions, it is necessary to use a very thin target (of thickness $\sim 100\,\mu g/cm^2$) as done in the present case. Otherwise, the time-of-flight of a fission fragment would have been affected significantly due to large energy loss of the fission fragments.

It may be noted that a fissioning nucleus having excitation energy ~ 40 MeV will most likely evaporate neutrons before scission. Therefore the mass of the fissioning system which has been assumed to be equal to m_{CN} may not be accurate. In fact, a theoretical calculation shows that the average neutron multiplicity for the system $^{19}F+^{238}U$ at ~ 40 MeV excitation energy is ~ 1.8. So, the fission fragment mass distribution was re-obtained after incorporating the pre-scission neutron evaporation correction taking mass of the fissioning nucleus as $m_{CN} - 2$. The results were found to be almost identical except an overall shift in the mass distribution of 1 u towards the left. The shift is negligible compared to the mass resolution of the present measurement which is ~ 5 u. Therefore, the uncertainty introduced in the mass distribution due to pre-scission neutron evaporation is insignificant.

5 Summary

We have described the design, development and performance optimization of two large area compact multiwire proportional counters for the measurement of fission fragments. The detectors have

2020 JINST 15 P02008

been tested successfully for their performance both offline and online fission sources. Two fast preamplifiers, based on Monolithic Microwave Integrated Circuits and transistors, were designed and developed for processing the negative anode signal and positive (x and y) position signals. Position resolution measured using an aluminium mask, was found to be ~ 1.3–1.4 mm. Time dispersion from the detector as well as from the electronics setup was found to be ~ 1.6 ns. After obtaining satisfactory performance results using radioactive ^{252}Cf fission source, the detectors were used in an in-beam experiment for measuring fission fragments produced in the ^{19}F + ^{238}U reaction. The time correlation spectra obtained from the timings of two anode pulses provide a clean separation of fission events from elastic and quasi-elastic events. Typical results for mass-distribution and folding angle distribution obtained in ^{19}F+^{238}U reaction were obtained from the analysis of the measured data and found to be consistent with the theory.

Acknowledgments

The financial support of BRNS through the Project No. 2012/21/11-BRNS/1090 is greatly acknowledged. We thank Dr. A. Saxena and Dr. S. Kailas for their encouragement and support during the course of this work. We also thank P. Patil, R. Gandhi and S.T. Sehgal for their help during detector testing.

References

[1] A. Pal et al., *Determination of $^{238}Pu(n, f)$ and $^{236}Np(n, f)$ cross sections using surrogate reactions*, *Phys. Rev.* **C 91** (2015) 054618.

[2] A. Pal et al., *Projectile-breakup-induced fission-fragment angular distributions in the $^{6}Li + ^{232}Th$ reaction*, *Phys. Rev.* **C 96** (2017) 024603.

[3] A. Pal et al., *Mass distributions of fission fragments from nuclei populated by multinucleon transfer or incomplete fusion channels in $^{6,7}Li + ^{238}U$ reactions*, *Phys. Rev.* **C 98** (2018) 031601.

[4] A. Pal et al., *Measurement of incomplete fusion cross sections in $^{6,7}Li + ^{238}U$ reactions*, *Phys. Rev.* **C 99** (2019) 024620.

[5] K. Hirose et al., *Role of Multichance Fission in the Description of Fission-Fragment Mass Distributions at High Energies*, *Phys. Rev. Lett.* **119** (2017) 222501.

[6] D. Ramos et al., *First Direct Measurement of Isotopic Fission-Fragment Yields of ^{239}U*, *Phys. Rev. Lett.* **123** (2019) 092503 [arXiv:1909.09447].

[7] G. Kessedjian et al., *Neutron-induced fission cross sections of short-lived actinides with the surrogate reaction method*, *Phys. Lett.* **B 692** (2010) 297.

[8] J.E. Escher, J.T. Burke, F.S. Dietrich, N.D. Scielzo, I.J. Thompson and W. Younes, *Compound-nuclear reaction cross sections from surrogate measurements*, *Rev. Mod. Phys.* **84** (2012) 353.

[9] G. Charpak, R. Bouclier, T. Bressani, J. Favier and C. Zupancic, *The Use of Multiwire Proportional Counters to Select and Localize Charged Particles*, *Nucl. Instrum. Meth.* **62** (1968) 262.

[10] A. Breskin, *Progress in low-pressure gaseous detectors*, *Nucl. Instrum. Meth.* **196** (1982) 11.

[11] A. Breskin et al., *Low-pressure multistep detector for very low energy heavy ions*, *Nucl. Instrum. Meth.* **221** (1984) 363.

2020 JINST 15 P02008

[12] D. Biswas et al., *Fission fragment velocity distribution measurement using time of flight technique*, *Nucl. Instrum. Meth.* **A 901** (2018) 76.

[13] T.K. Ghosh, S. Pal, T. Sinha, S. Chattopadhyay, K.S. Golda and P. Bhattacharya, *Time of flight (TOF) spectrometer for accurate measurement of mass and angular distribution of fission fragments in heavy ion induced fission reactions*, *Nucl. Instrum. Meth.* **A 540** (2005) 285.

[14] A. Jhingan et al., *Compact multiwire proportional counters for the detection of fission fragments*, *Rev. Sci. Instrum.* **80** (2009) 123502.

[15] K.D. Schilling et al., *The Dübna double-arm time-of-flight spectrometer for heavy-ion reaction products*, *Nucl. Instrum. Meth.* **A 257** (1987) 197.

[16] M. Ahmad et al., *A time-of-flight telescope for charged particles produced in neutron-induced reactions*, *Nucl. Instrum. Meth.* **A 228** (1985) 349.

[17] A. Arefiev et al., *Parallel plate chambers: a fast detector for ionizing particles*, *Nucl. Instrum. Meth.* **A 348** (1994) 318.

[18] D. Swan et al., *A simple two-dimensional PPAC*, *Nucl. Instrum. Meth.* **A 348** (1994) 314.

[19] H. Kumagai et al., *Delay-line PPAC for high-energy light ions*, *Nucl. Instrum. Meth.* **A 470** (2001) 562.

[20] C. Delaney et al., *Rise and plasma times in semiconductor detectors*, *Nucl. Instrum. Meth.* **A 215** (1983) 219.

[21] V.E. Viola, K. Kwiatkowski and M. Walker, *Systematics of fission fragment total kinetic energy release*, *Phys. Rev.* **C 31** (1985) 1550.

2020 JINST 15 P02008